ISSN: 0976-3031

Available Online at http://www.recentscientific.com

CODEN: IJRSFP (USA)

International Journal of Recent Scientific Research
Vol. 9, Issue, 4(E), pp. 25812-25821, April, 2018

International Journal of Recent Scientific Research

DOI: 10.24327/IJRSR

Research Article

A HYBRID RETINAL IMAGE SEGMENTATION AND CLASSIFICATION APPROACH FOR DIAGNOSIS OF DIABETIC RETINOPATHY

Ashok Kumar, D[1]* and Sankari, A[2]

[1]Department of Computer Science, Government Arts College, Trichirappalli-620 022
[2]Department of Computer Science, Research Scholar, Bharathidhasan University, Trichirappalli-620 022

DOI: http://dx.doi.org/10.24327/ijrsr.2018.0904.1936

ARTICLE INFO

Article History:

Received 8th January, 2018
Received in revised form 21st February, 2018
Accepted 05th March, 2018
Published online 28th April, 2018

Key Words:

Diabetic Retinopathy, Hit-or-Miss Transformation (HMT), Morphological Operations, Scanning Window Analysis (SWA), Difference Subspace Sparse representation based Classification (DSSRC).

ABSTRACT

Efficient segmentation and classification of the retinal image enables accurate diagnosis of the Diabetic Retinopathy at the early stages. This prevents the vision loss of the patients. Existing edge detection techniques could not accurately segment the fundus images due to the presence of noise and high-frequency contents. This paper proposes a Hybrid Morphological-based Scanning Window Analysis and Hit-or-Miss Transformation (HMSWA-HMT) and Difference Subspace Sparse representation based Classification (DSSRC) approach to segment and classify the retinal image, for the efficient diagnosis of Diabetic Retinopathy. The morphological operators are applied to minimize the noise or enhance the image. The SWA method provides better localization irrespective of the complex disorder patterns in the image. The HMT detects the significant points such as bifurcations points, ridge and vessel ends that are able to define the vascular skeleton. The Difference Subspace Sparse representation based Classification (DSSRC) method focuses on improving the distinguish ability for the classes rather than the representation capability for the samples. From the experimental analysis, it is observed that the proposed HMSWA-HMT approach achieves better performance in terms of accuracy, sensitivity, true positive rate and specificity and requires minimum time complexity than the existing segmentation and classification techniques.

INTRODUCTION

Diabetic retinopathy (DR) occurs due to the damage of small blood vessels in the retina through the leakage of fluid or hemorrhage, due to the increase in the blood sugar levels. The DR causes vision impairment and blindness among the patients suffering from diabetes mellitus. It is the major cause of blindness in the people aged from 20-64. The DR affects almost 3.4 percent of the population. There is a steady increase in the population affected by DR to 126.6 million in 2010. By 2038, it will rise to 191.1 million [1]. Among them, nearly one-fourth have vision-threatening disease that causes severe damage to the retina or vision loss. The DR is classified into two types such as Proliferative DR (PDR) and non-PDR (NPDR). The DR remains undiagnosed until it causes severe retinal image. Mostly, a few blood spots may spread over the visual field and disappear after a few hours. Hence, the patients could not able to recognize any symptoms at the early stage of DR. After few days, the blood vessels will start to bleed without any prior symptoms and causes complete vision loss in the patients. The precipitation of the plasma protein in the retinal region causes formation of the bright lesions such as hard exudates and cotton wool spots. The bright lesions look like bright, reflective, white or cream-colored lesions on the retinal images. The segmentation of the bright lesions in the retinal images facilitates the automatic screening of the DR. To identify the severity of the DR, it is necessary to detect the bright lesions [2]. Automatic detection of the bright lesions caused by the DR is essential to avoid the loss of vision. The detection of bright lesions can be predicted using effective image processing algorithms for detecting the severity of the disease.

Various schemes for the segmentation of the retinal blood vessel and classification of the retinal images based on the type and severity of the diseases are developed [3-10]. Nayak *et al*. [11] proposed a method for the automatic classification of retinopathy based on the Artificial Neural Network (ANN) for the early detection of the DR. The existing methods enable accurate detection of DR at the early stages. However, these

Corresponding author:* **Ashok Kumar, D
Department of Computer Science, Government Arts College, Trichirappalli-620 022

techniques require high computational complexity and large training to the classifiers [12]. Detection of the significant points such as terminal, intersection and bifurcation points provides information about the vascular structure and facilitates efficient diagnosis of the retinal disease [13].

This paper proposes a hybrid retinal image segmentation and classification approach. The input image is enhanced for removing the unwanted distortions. A hybrid method of H-MSWA-HMT is applied for the segmentation of image. To remove the spurs from the edges in the retinal image, the SWA is combined with the morphological operations. It is utilized for the optical point of convergence. The optimal features are obtained from the segmented image. The DSSRC is applied for the classification of the retinal images into normal (MA) and abnormal (non-MA) images.

The main contributions of the proposed work are

- Detection of the significant points in the retinal vascular tree.
- Segmentation of the ridge end, bifurcation points and vessel ends from the image.
- Extraction of optimal features from the segmented image.
- Classification of the retinal image into normal and abnormal images by using the optimal features.

The detection of significant points in the retinal vascular tree increases the information about the vascular structure allowing its use for medical diagnosis. In this work, three types of relevant points such as end points, bifurcations and crossing points are distinguished. The end points define the beginning and the end of a retinal blood vessel. Bifurcations represent the joining points and separating points of two different blood vessels. The crossing point represents two different overlapping vessels located in different planes. This helps in the identification of arteriovenous nicking and diagnosis of hypertension.

The sections in the manuscript are systematized in the following order: Section II describes an overview of the prevailing retinal image segmentation techniques. Section III explains the proposed work including HMSWA-HMT based image segmentation and DSSRC-based classification approach. Section IV illustrates the comparative analysis of the proposed work and existing classification techniques using the benchmark datasets. The concluding statements of the proposed work are discussed in Section V.

Existing Image Segmentation Approaches

Nguyen *et al*. [14] suggested a method for finding the blood vessels from the retinal images in an automatic way based on the line detection method. Accurate segmentation on the central reflex vessels is achieved while ensuring the efficient separation of the close vessels. Chen *et al*. [15] presented a novel approach for the segmentation and registration of the retinal image. The false detection is prevented through the hypothesis testing. Chauhan and Gulati[16] described the method for extracting the cup to optic disc ratio from the retinal images. The OTSU histogram is applied for the efficient segmentation of the optic disc and cup. Karimi and Pourghassem[17] proposed a method for the segmentation of the optical disk (OD) based on the spatial density of the grayscale pixels. The thresholding and averaging methods are used for detecting and differentiating the OD segments. The proposed method achieved high accuracy rate on the DRIONS and DRIVE datasets. Li *et al*. [18] presented a cross-modality learning based approach for the segmentation of vessel in the retinal image. A wide and deep NN with strong induction capability is proposed for modeling the transformation, and an efficient training strategy is presented. The proposed approach does not require any artificially designed feature and preprocessing step. The impact of subjective factors is reduced.

Odstrcilik *et al*. [19] suggested a novel method for the segmentation of blood vessels with varying diameters in the high-resolution color fundus images. The novel segmentation method yielded maximum segmentation accuracy than the state-of-the-art methods. Zhao *et al*. [20] introduced a novel segmentation method based on the level set and region growing technique. High segmentation accuracy on the DRIVE and STARE databases is achieved. Azzopardi and Petkov[21] used a set of keypoint detectors for the detection of bifurcations in the segmented retinal images. The proposed filter achieved high precision and recall. Jiang *et al*. [22] proposed a fuzzy-based algorithm for the efficient segmentation of retinal blood vessel. The fuzzy-based clustering is applied on the texture features for the segmentation of blood vessel based on the local gray value entropy. The algorithm achieved better performance in terms of sensitivity, Receiver Operating Characteristic (ROC) curve and specificity.

Franklin and Rajan[23] developed an ANN based technique for the automatic segmentation of vessels in the fundus image. The proposed technique provided knowledge about the location of vessel for ensuring better screening of the DR. Orlando and Blaschko[24] presented a new method for the segmentation of blood vessel in the fundus images based on the conditional random field model. Mahapatra[25] proposed a new approach for combining the multiple annotations for image segmentation by utilizing the semi supervised learning approach and graph cut method. Accurate segmentation of the retinal image is achieved. Zhang *et al*. [26] presented an automatic filter-based approach based on the three-dimensional for the segmentation of retinal vessel. The LAD-OS is highly capable of dealing with crossings, closely parallel and tiny vessels and central arterial reflex. The improved computational speed of the filter-based approach has ensured better processing of the large datasets.

Proposed Work

The images obtained from the DIARETDB1 [27] database is applied as input to the preprocessing step. The image enhancement is applied as a preprocessing technique for eliminating the unwanted distortion present in the retinal image. A hybrid method of morphological-based Scanning Window Analysis and Hit-or-Miss Transformation (H-MSWA-HMT) is applied for the segmentation of image. After segmenting the ridge end, bifurcation points and vessel ends in the retinal image, the optimal features are extracted from the segmented image. The difference Subspace Sparse representation based Classification (DSSRC) is applied for the classification of the retinal images into normal (MA) and abnormal (non-MA) images. Due to the segmentation of the ridge end, bifurcation points and vessel ends and extraction of

the optimal features, the normal and abnormal images are classified efficiently. This facilitates the efficient diagnosis of the DR. Fig.1 shows the overall flow diagram of the proposed work.

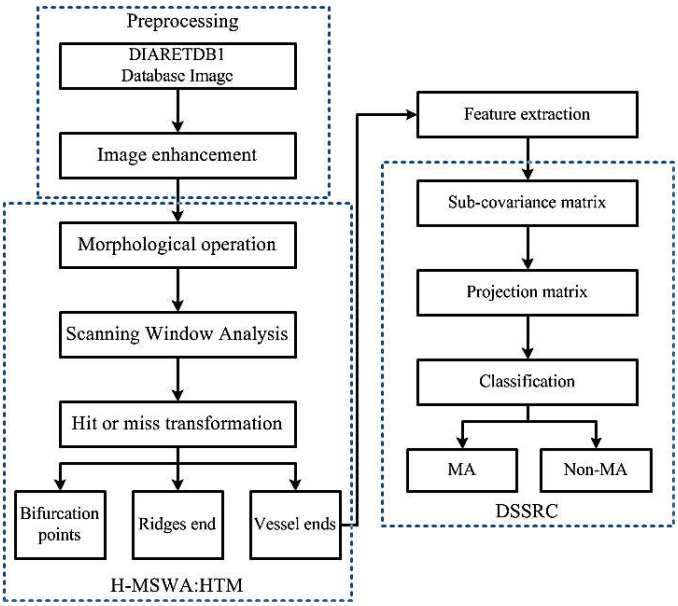

Fig 1 Overall flow diagram of the proposed work

Image enhancement

Image enhancement is a process for removing the unwanted distortion due to the decrease in the contrast, noise, inappropriate intensity saturation, blurring effect, etc., and determining the hidden information contained in the images [28, 29]. The decline in the image quality of the ocular fundus image occurs due to the factors such as media opaqueness, defocus or vicinity of relic [30, 31]. Image enhancement improves the quality of the images to be suitable for analysis, processing or viewing. The image histogram represents the distribution of pixel intensity in an image, in a graphical format and determines the rate of occurrence of the gray levels in the image. The horizontal line of the graph denotes the possible gray level in the images and horizontal line represents the number of occurrence of the gray level pixels. In a dull or brightest image, the gray level will be clustered to the limits of the histogram. In the versatile differentiated image, these gray levels will spread out over the significant regions. In the histogram equalization technique, the image intensity is adjusted so as to match the histogram of the output image with a specific histogram. This leads to the increase in the contrast level of the image. The pixel values of the output image are distributed uniformly throughout the specific range. The adaptive histogram equalization is applied for enhancing the contrast in the input image. The input image of the retina is illustrated in Fig.2. Fig.3 shows the green plane and Fig.4 illustrates the histogram equalized image.

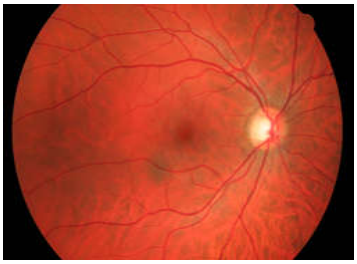

Fig 2 Input image

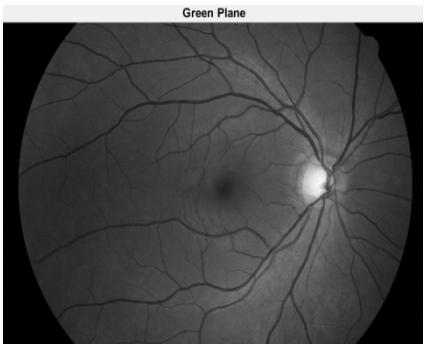

Fig 3 Green plane

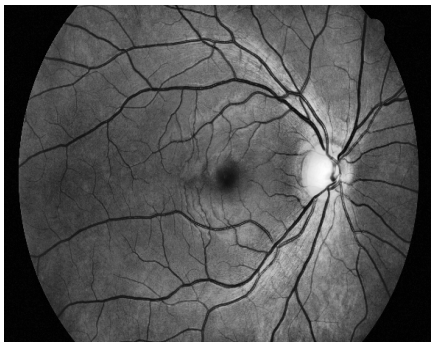

Fig 4 Histogram equalized image

Image segmentation

Segmentation process divides the whole image into multiple subsections for analyzing the region of interest (ROI) in the image. The segmentation process is stopped, when the object of interest is found. The segmentation is done based on the presence of discontinuities such as edges and similitudes in the image. Thresholding permits the splitting of an image into foreground and background by converting it into a binary image. It includes separation of the image into white or dark pixels by comparing the value of pixels with the threshold level. If the pixel intensity is found to be greater than the threshold value, it is considered as white pixel. If the pixel intensity is lesser than the threshold value, it is fixed as black pixel. The black pixel indicates the background and white pixel indicates the foreground. The thresholding procedure is highly beneficial for avoiding the futile subtle element and highlighting the region of interest. Edges contain the highly substantial data in an image. The edges are utilized to observe and isolate the objects. An edge in an image involves a visible distinction in the pixel values lying inside a specific range. The size of the rise in the pixel values is discovered for the edge recognition calculations. The Sobel edge detector [32] applies a couple of 3×3 convolution masks for evaluating the angles and slope in the X-direction and Y-direction, respectively.

MSWA

Morphology is highly suitable for the analysis or detection of shapes in the images. Erosion and dilations are the two main morphological procedures [33]. The dilation adds the pixels to the boundary of objects in the image and erosion removes the pixels from the boundaries. The opening process is the structured removal of boundary pixels in the image region and closing is the structured filling of the boundary pixels. The objects in the image are processed based on its shape characteristics. Usually, the size of the structuring element is 3×3. The structuring element is initially located at the center

pixel and shifted over the image. The structuring elements are compared with the set of original pixels. The pixel lying below the origin of the structuring element is set to 1, based on the matching of double sets of structuring elements with the specific condition determined by the morphological operator. Otherwise, the pixel value is fixed to zero. These morphological operators are used for selecting or suppressing the features of certain shape or selecting the objects with a particular direction. The more refined operators consider zeros, ones and don't care's in the structuring element. The morphological operators can also be applied to gray level images to reduce noise or enhance the image.

SWA

The SWA is used to stimulate the characteristics after setting the thinned image to a single pixel [33]. Similarly, all the lines are reduced to one pixel. A 3×3 window is used for obtaining the information about the ridges and bifurcation. The thinned image is scanned from the top to bottom and left to the right by using the window. If the center pixel is found to be black, the presence of any ridges or bifurcation is detected. Hence, it is clear that only two pixels in the scanning window result in the end of the ridges. If the pixel count is greater than or equal to four, it leads to be a bifurcation. The scanning window of 70×70 is used for the localization of optical focal point. The SWA method provides better localization irrespective of the complex disorder patterns in the image. This minutiae information is used for the recognition purpose.

Hit-or-miss transformation (HMT)

The HMT process is applied for discriminating the exact patterns in a binary image [34]. It is applied for detecting the significant points on an image by examining the image with a set of structuring element. The structuring element comprises two elements B_{FG} representing the set of pixels that match with the foreground and B_{BG} defining the set of pixels matching with the background. Both the background and foreground structuring elements are separate sets and they share the same origin, i.e., $B_{FG} \cap B_{BG} = 0$. The HMT determines whether the origin belongs to the $B_{FG}\ and\ B_{BG}$[35]. The HMT of a set 'X' by a complex structuring element $B = (B_{FG}, B_{BG})$ is described as [13]

$$HMT_B(X) = \epsilon_{B_{FG}}(X) \cap \epsilon_{B_{BG}}(X^c) \quad (1)$$

Where X^c is the complement set of X.

Terminal and bifurcation points

The HMT is applied to the skeleton for detecting the terminal and bifurcation points by using multiple structuring elements. The foreground pixel is indicated by ones and background pixel is indicated by zeros. The structuring element is used in the orientations of the $B_{FG}\ and\ B_{BG}$. Totally, eight hit-or-miss iterations and 16 structuring elements are used for detecting the terminal and bifurcation points, respectively. The shape of the structuring element is related to the topology of the point. There will be a single neighbor for any terminal point surrounded by the background pixels. A bifurcation point requires three neighbors in the particular positions.

Retinal skeleton is defined as a single-pixel dense structure that is completely eight-connected. The multiple paths that are essential in this type of eight-connectivity should be avoided, when the significant points belong to the skeleton. Before detecting the terminal and bifurcation points, there is a need to convert the connectivity of the skeleton from 8 to 'm', to remove the multiple paths [34].

A pixel 'p' includes four horizontal and vertical neighbors $N_4(p)$ and four diagonal neighbors $N_D(p)$. All neighbors are represented as eight-neighbors $N_8(p)$. Two binary pixels 'p' and 'q' are 8-connected, if 'q' is in the set $N_8(p)$. The binary pixels are m-connected if

- The binary pixel 'q' is in $N_4(p)$ or
- 'q' is in $N_D(p)$ and $N_4(p) \cap N_4(q) = 0$.

In the eight-connectivity case, multiple paths are established in four basic patterns. The HMT enables detection of all basic patterns. Then, the central pixels should be changed to zero for eliminating multiple paths. The transformation from eight to 'm' connectivity is achieved through a specific order of morphological steps

$$\Theta_1(X, B_{3_1}) = X - HMT_{B_{3_1}}(X) = X \cap \left[HMT_{B_{3_1}}(X)\right]^c \Theta_2(\Theta_1, B_{3_2}) \quad (2)$$

$$= \Theta_1 - HMT_{B_{3_2}}(Y_1) = Y_1 \cap \left[HMT_{B_{3_1}}(Y_1)\right]^c \Theta_3(\Theta_2, B_{3_3}) \quad (3)$$

$$= \Theta_2 - HMT_{B_{3_3}}(Y_2) = Y_2 \cap \left[HMT_{B_{3_3}}(Y_2)\right]^c \Theta_4(\Theta_3, B_{3_4}) \quad (4)$$

$$= \Theta_3 - HMT_{B_{3_4}}(Y_3) = Y_3 \cap \left[HMT_{B_{3_4}}(Y_3)\right]^c \Theta(X, B_3\ ) \quad (5)$$

$$= \Theta_4 \quad (6)$$

Where 'X' represents the input image that contains eight-connected skeleton and Θ denotes the output image with the m-connectivity skeleton [13].

Crossing points

Due to the presence of intersection between different branches of the vascular tree, the HMT process could not be able to detect the pattern recognition of the skeleton. It is applied only in the detection of simple crossing point. The branches in the vascular tree do not overlap in only one pixel, so many crossing points are not simple. Multiple points can belong to the similar intersection. As there are three neighbors for the extremes of the crossing, it is set as bifurcation. The characteristic patterns of the bifurcation points are achieved.

In the existing works, the crossing points of the vessel are considered as two bifurcation points that are located too close to each other. Therefore, a circular window of predefined size is focused on the target bifurcations. If there are four intersections between the window and skeleton, the point is marked as a crossing. The crossing points are detected depending on the size of window. If the window size is too big, the vessels that do not belong to the crossing point can overlap with the window. The crossing points are not detected, if the window size is too small. The size of the intersections varies from one case to another. Also, the size depends on the image resolution.

The origin of the retinal vessels lies in the head of optic disk. The vessels separate from this center point to form the retinal vascular tree structure. The arteries and veins overlap in a certainregion and generate the crossing points. This means that during intersection of the arteries and veins, a closed loop is

generated due to the common origin of the vessels. This closed loop is used for differentiating a crossing point. Based on the idea, a novel algorithm is proposed for analyzing all the points that are initially detected as a bifurcation to discriminate them as really crossing points.

A bifurcation point is accounted as a crossing point, when a circular-shaped window is centered on this bifurcation point. Four or more intersections exist between the circular window and skeleton. The radius of the window is thrice the average diameter of the blood vessels. If the candidate point is a part of the close loop, the nearby point to the crossing point is observed. If the nearby point is directly connected with the previous point and it is not a part of the same loop, both are called as crossing points [13].

Input: Image of the retinal skeleton 'f', circular window 'W'
Output: Binary image of the terminal points f_{TP}, binary image of bifurcation points f_{BP} and binary image of the crossing points f_{CP}

Initialize B_1, B_2, B_3, B_4

$f_m \leftarrow \Theta_{B_3}(f)$m-connectivity conversion;
$f_{TP} \leftarrow \mathrm{HMT}_{B_1}(f_m)$terminal point detection;
$f_{BP} \leftarrow \mathrm{HMT}_{B_2}(f_m)$bifurcation point detection;
$f_{CP_1} \leftarrow \mathrm{HMT}_{B_4}(f_m)$crossing point detection;
Complex crossing point detection
for i ← 1 to $\sum(f_{BP})$ ***do***
if $\sum(W_{BP_i} * f_m) \geq 4$ ***then***
if $f_{BP_i} \in close\ loop$ ***then***
$f_{BP_i} \leftarrow$
$\arg\min\left(dist\left(f_{BP_i}, f_{BP}\right)\right)$;

if $\left(f_{BP_i} is\ connected\ with\ f_{BP_j}\right) \& \left(loop\ \left(f_{BP_i}\right) \neq loop\ \left(f_{BP_j}\right)\right)$ ***then***
$f_{CP_{2_i}} = f_{BP_i} + f_{BP_j}$;
end
end
end
end

$f_{CP} = f_{CP_1} + f_{CP_2}$ crossing point detection;

The significant points are used as biometric features, benchmarks or key points for finding the branching patterns. Multiple main orientations are estimated at each pixel by analyzing the image block.

Let $f(x): E \rightarrow \mathbb{R}$ be a gray-level image, where the support space is $E \subset Z^2$ and pixel coordinates are $x = (x, y)$. The absolute value of the gradient of $f(x)$represented as $g(x)$ is described below

$$g(x) = \|\nabla f(x)\| = \sqrt{\left(\frac{\partial f(x,y)}{\partial x}\right)^2 + \left(\frac{\partial f(x,y)}{\partial y}\right)^2} \quad (7)$$

The directional opening of$g(x)$value is represented as the directional erosion of 'g' by a linear structuring element of length 'l' and direction 'θ'. The directional erosion operation is followed by the directional dilation.

$$\gamma L^{\theta,l(g)(x)} = \delta_{L^{\theta,l}}\left[\varepsilon_{L^{\theta,l}}(g)\right](x) \quad (8)$$

$$\varepsilon_{L^{\theta,l}}(f)(x) = \wedge_{h \in L^{\theta,l(x)}}\{f(x+h)\} \quad (9)$$

$$\delta_{L^{\theta,l}}(f)(x) = \vee_{h \in L^{\theta,l(x)}}\{f(x-h)\} \quad (10)$$

The orientation model depends on the breakdown of the gradient information by the group of linear openings, $\{\gamma L^{\theta,l}\}_{i \in I}$ according to the definite discretization of the orientation space $\{\theta_i\}_{i \in I}$. The filtering process distributes the information about the orientation. This avoids the mismatch of the angle due to noise. The sampling process of the Gaussian low-pass filter is denoted by the kernel H_σ as described below

$$H_\sigma(\omega_1, \omega_2) = e^{-\frac{\sigma^2\left(\omega_1^2 + \omega_2^2\right)}{2}} \quad (11)$$

Where σ denotes the spatial standard deviation of the filter. The directional signature at the pixel '**x**' is defined as

$$s_{x;l}(i) = \tilde{g}_{\theta_i}(x) \quad (12)$$

The signature is included using the cubical b-splines. The maximum limit of the directional signature corresponds to the multiple orientations at the pixel 'x'. The orientations at all pixels are collected to offer the multidimensional vector field $\vec{\theta}(x)$.

An interior point is chosen as a representative of each branch. The orientation vector of the interior point defines the orientation of the branch at this pixel. A circular window is located at each bifurcation point to find the interior points. The crossing between the window and vascular skeleton of the branch is chosen. The choice of this pixel is not critical, due to the slow variation in the orientation vector field inside the vessel. The Anisotropic Morphological Filters [36] is applied for estimating orientation lying between $-90°$ and $90°$. The direction of each vector is obtained by considering the location of the pixel representing each branch with respect to the center of the bifurcation. The direction of the vector is obtained by considering the quadrant of the representative pixel and a vector field defined between $0°$ and $360°$ is provided. The angular difference between the branches in the circular window can be computed, after converting the orientation space [13].The detection of optic discand blood vessel is depicted in Fig.5 and Fig.6 respectively. The input image overlaid with the detected blood vessel is presented in Fig.7. Fig.8 shows the blood vessel end point detection. The ends of the blood vessels are indicated with the red color. The detection of the crossover point and bifurcation point is depicted in Fig.9 and Fig.10 respectively.

Fig 5 Optic disc detection

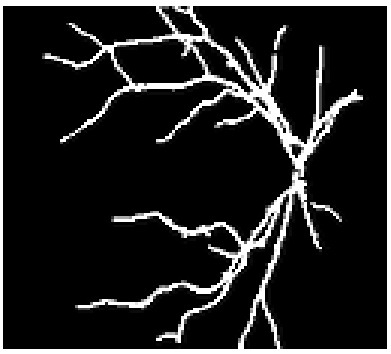

Fig 6 Blood vessel detection

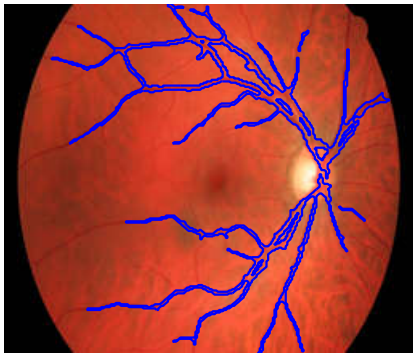

Fig 7 Input image overlay with blood vessel

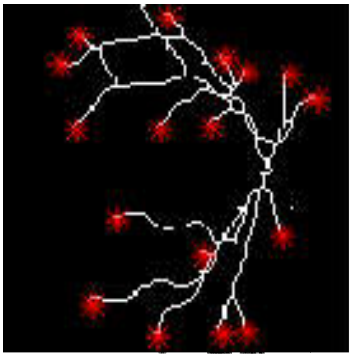

Fig 8 Blood vessel end point detection

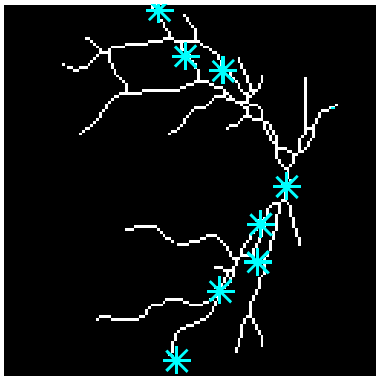

Fig 9 Crossover point detection

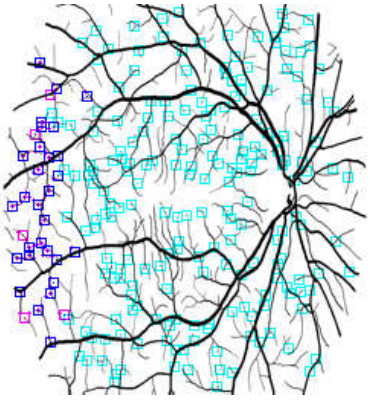

Fig 10 Bifurcation point detection

Feature extraction

Feature extraction is the process of discovering best features to be used for the classification tasks. It directly influences the effectiveness of the classification task [37]. Features such as shape, color, intensity, texture, etc., are used for describing the content of the retinal image. In this work, totally 27 features are extracted from the segmented image. Among them, 12 optimal features are considered. The features are number of bifurcation points, total area, mean and deviation, circularity mean, circularity deviation, distance from center mean, distance from center deviation, optic distance, ridges end, bifurcation points, vessel ending and bifurcations. Fig.11 shows the final extracted features in the retinal image.

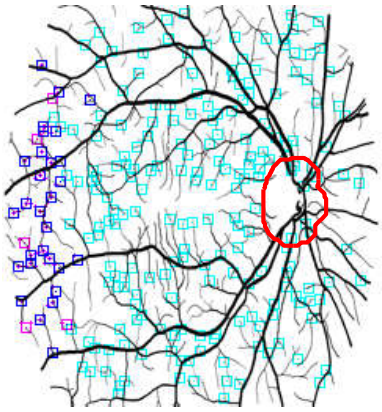

Fig 11 Final extracted features

Image Classification

The optimal features are applied as input to the classifier. Due to the extraction of the optimal features, the normal and abnormal images are classified efficiently. This facilitates the efficient diagnosis of the DR.

SRC

Let us suppose that there are 'n' number of training samples from 'c' classes. Each class 'i' includes n_i training samples, such that $n = \sum n_i$. Each image sample is transformed to the vector. The j[th] sample from the i[th] class is indicated as x_i^j. The linear integration of the training samples represents the probe image 'y' [38].

$$y = XA \tag{13}$$

Where $X = \left[x_1^1, x_1^2, \ldots, x_c^{n_c}\right]$, The sample matrix 'A' is solved by

$$A = \arg\min(\|y - XA\|_2^2 + \mu\|A\|_1) \quad (14)$$

Where μ is the parameter and $\| \ \|_1$ denotes the l_1 norm of a vector. The coding error of each class is derived while obtaining the coefficient vector,

$$\|y - X_i A_i\|_2^2, \ where \ i = 1, 2, \dots c \quad (15)$$

Where $X_i = [x_i^1, x_i^2, \dots, x_i^{n_i}]$ and A_i is the coefficient vector for the class 'i'. The probe image is assigned to the class that reduces the coding error.

DSSRC

In the DSSRC process, the separability of the subspaces covered by the samples from specific class is maximized. If the training samples from 'c' classes are given, the difference subspace from the training samples should be learned. The covariance matrix of the class 'k' is denoted as

$$C_k = \sum_{i=1}^{n_i} x_k^i x_k^{iT} \quad (16)$$

The sum covariance matrix is denoted as

$$G = \sum_{j=1}^{c} C_j \quad (17)$$

It is proven that the Eigen vectors are the basis of the difference subspace of 'c' subspaces that are traversed by the training samples from a specific class. The Eigen vectors correspond to the Eigen values lesser than 1. There is a need for choosing the number of subspace dimensionality in the subspace learning technique. The Fisher criterion is used to determine the optimal dimensionality of the subspace. Fig.12 illustrates the geometric interpretation of difference subspace.

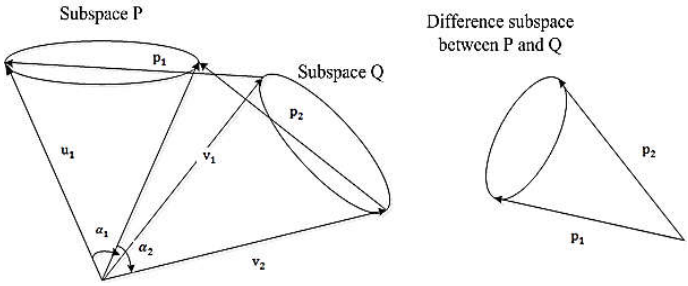

Fig 12 Geometric interpretation of difference subspace

While obtaining the difference subspace projection $W = [p_1, p_2, \dots]$, all the training samples $W^T x_1^1, W^T x_1^2, \dots, W^T x_c^{n_c}$ are projected into the difference subspace. $W^T y$ represents the testing samples. The direct combination of the training samples represents the testing sample, in this subspace. The combination coefficient vector in the subspace is sparse.

$$W^T y = W^T X B \quad (18)$$

To obtain the sparse combination coefficient vector, there is a need to solve the problem

$$B = \arg\min\|W^T y - W^T X B\|_2^2 + \mu\|B\|_1 \quad (19)$$

The similar classification criterion is applied in the DSSRC. When the linear coefficient vector 'B' is obtained, the coding error of $W^T y$ by each class is derived by

$$\|W^T y - W^T X_i B_i\|_2^2, \ where \ i = 1, 2, \dots, c \quad (20)$$

Where B_i is the coefficient vector for the class 'i'. The testing sample 'y' can be assigned to the class that reduces the coding error in difference subspace. The DSSRC algorithm is given as follows

DSSRC Algorithm

Input: Training and testing samples
Step 1: Calculate the sum covariance matrix
Step 2: Obtain the Eigen vectors p_i of the sum covariance matrix and use 'W' as the projection matrix
Step 3: Project all the training samples by the matrix 'W' and solve the optimization problem
Step 4: Classify the testing samples into the class that reduces the coding error $\|W^T y - W^T X_i B_i\|_2^2, \ where \ i = 1, 2, \dots, c$

The proposed method is highly efficient in representing the difference among the subspaces. The canonical vectors describe the additional information about the difference between two subspaces. In this method, the pair of samples from different classes does not contribute to the sum covariance. Hence, two samples in the difference subspace can be classified easily. The DSSRC method requires lower computational complexity.

Performance Analysis

The proposed HMSWA-HMT is evaluated using the DRIVE [39] and compared with the method proposed by Calvo *et al*. [40] and HMT [13]. The experimental analysis is carried out using the Matlab software. Fig.13 shows the comparative results of the True Positive Rate (TPR) or sensitivity, Positive Predictive Value (PPV) or precision, True Negative Rate (TNR) or specificity and Negative Predictive Value (NPV) for the method proposed by Calvo *et al*. [40], HMT [13] and proposed HMSWA-HMT, for detecting the bifurcation point. Calvo *et al*. method achieves the TPR of about 1.000 and PPV of about 0.908 for the detection of bifurcations and crossing points. The method proposed by the Calvo *et al*. yields high TPR and low TNR by detecting multiple false positives and negatives. The proposed method achieves better TPR, PPV and NPV and lower TNR than the HMT. Fig.14 illustrates the comparative analysis of the existing method proposed by Calvo *et al*., HMT and proposed HMSWA-HMT, for the detection of crossing point. The method proposed by Calvo *et al*. achieves maximum TPR and NPV of about 1. From the analysis graph, it is observed that the proposed method achieves better TPR, PPV and NPV and lower TNR than the HMT.

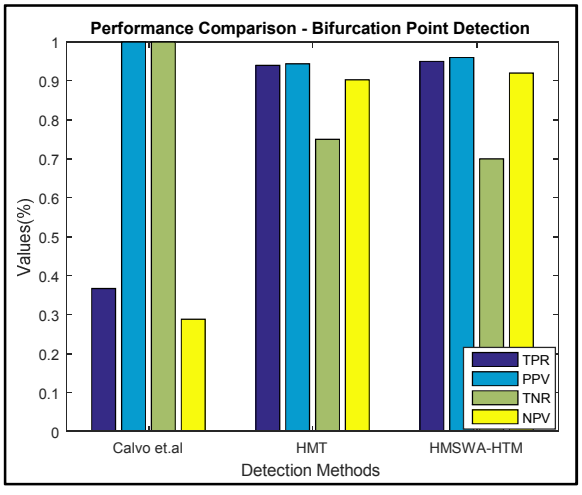

Fig 13 Comparative TPR, PPV, TNR and NPV results for bifurcation point detection

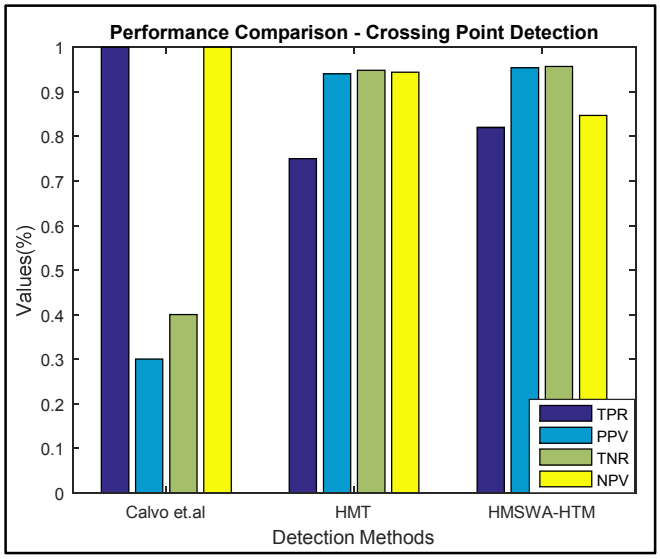

Fig 14 Comparative analysis of TPR, PPV, TNR and NPV for the detection of crossing point

The proposed method is compared with Sanchez *et al*. [41], Agurto *et al*. [42], Antal *et al* [43], Barriga *et al*. [44], DREAM [45] and HM-SPCA and evaluated using the MESSIDOR dataset [46]. Fig.15 depicts the comparative analysis of the sensitivity, accuracy rate and specificity for different image classification methods. The proposed HMSWA-HMT approach yields maximum sensitivity, specificity and accuracy rate than the existing classification methods. Due to the segmentation of the ridge end, bifurcation points and vessel ends and extraction of the optimal features, the normal and abnormal images are classified efficiently. This facilitates the efficient diagnosis of the DR.

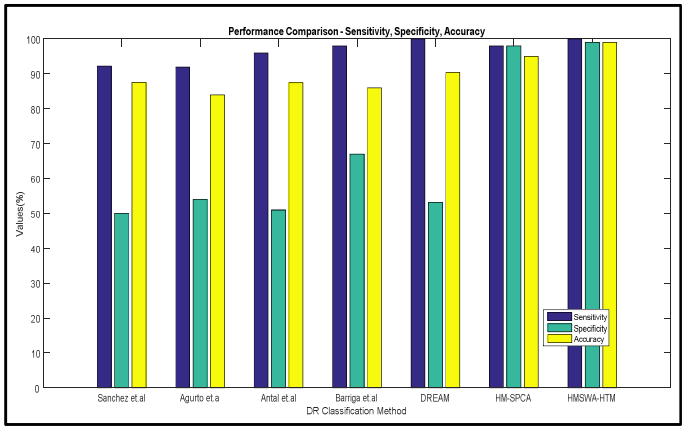

Fig 15 Sensitivity, specificity and accuracy analysis for different classification methods

The proposed method is compared with the retinal feature extraction approach [33]. Fig.16 shows the healthy image detection analysis. Fig.17 illustrates the Glaucoma image detection and Fig.18 presents the DR image detection. In the retinal image database, there are 25 healthy images, 15 Glaucoma images and DR images. Existing feature extraction method has extracted 25 healthy images, 14 Glaucoma images and 13 DR images. The existing method achieved accuracy of about 100%, 93.33% and 80% for the extraction of healthy images, Glaucoma images and DR images respectively. Our proposed method has successfully extracted 25 healthy images, 14 Glaucoma images and 14 DR images. The proposed method achieved accuracy of about 100%, 100% and 93.33% for the extraction of healthy images, Glaucoma images and DR images respectively.

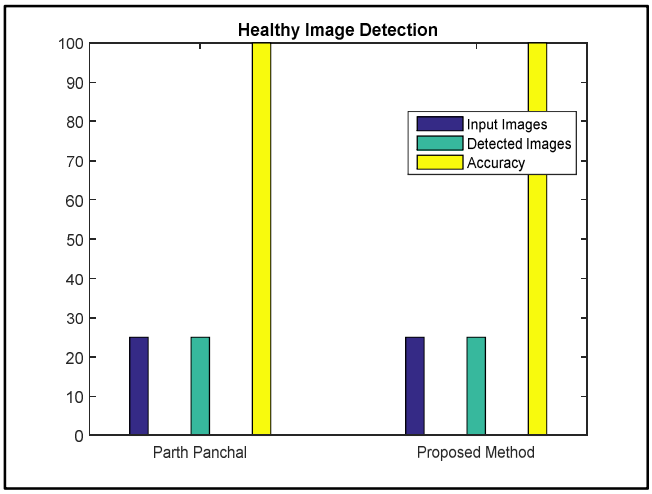

Fig 16 Healthy image detection

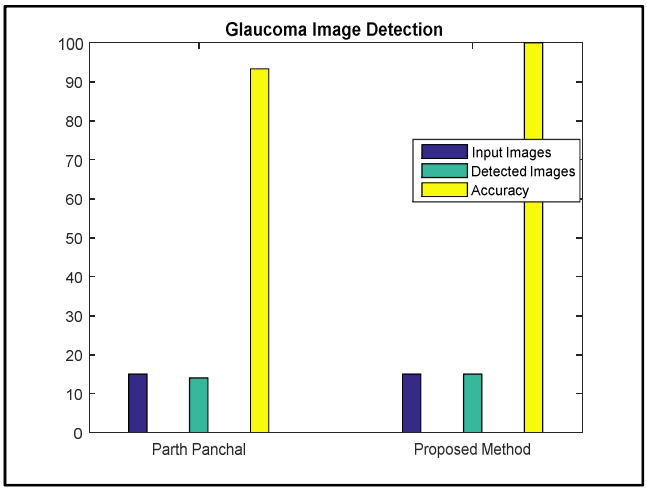

Fig 17 Glaucoma Image detection

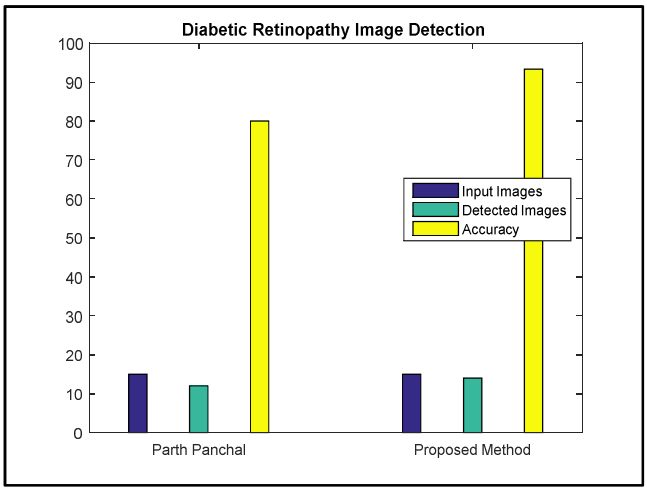

Fig 18 DR image detection

CONCLUSION

Identification of bifurcation, edges, crossing points and vessel ends in the retinal image is a tough task due to the complexity of the vascular network. There is a need to detect significant points such as bifurcation, crossing points and vessel ends of

the retinal network on the vessel centerline. This work proposes the application of HMT to detect the significant points. The morphological operation is combined with the SWA for eliminating the outgrowths from the edges in the retinal image. The optimal features are extracted and applied for the classification process. The proposed work is evaluated using the DRIVE and MESSIDOR datasets. The proposed HMSWA-HMT approach yields high sensitivity, true positive rate, specificity, accuracy and requires minimum time complexity than the existing techniques.

References

1. Y. Zheng, M. He, and N. Congdon, "The worldwide epidemic of diabetic retinopathy," *Indian journal of ophthalmology*, vol. 60, p. 428, 2012.
2. G. G. Yen and W.-F. Leong, "A sorting system for hierarchical grading of diabetic fundus images: A preliminary study," IEEE Transactions on Information Technology in Biomedicine, vol. 12, pp. 118-130, 2008.
3. A. M. Mendonca and A. Campilho, "Segmentation of retinal blood vessels by combining the detection of centerlines and morphological reconstruction," IEEE transactions on medical imaging, vol. 25, pp. 1200-1213, 2006.
4. M. M. Fraz, P. Remagnino, A. Hoppe, B. Uyyanonvara, A. R. Rudnicka, C. G. Owen, *et al*., "Blood vessel segmentation methodologies in retinal images–a survey," Computer methods and programs in biomedicine, vol. 108, pp. 407-433, 2012.
5. J. Nayak, P. S. Bhat, and U. Acharya, "Automatic identification of diabetic maculopathy stages using fundus images," *Journal of medical engineering & technology,* vol. 33, pp. 119-129, 2009.
6. K. Ram, G. D. Joshi, and J. Sivaswamy, "A successive clutter-rejection-based approach for early detection of diabetic retinopathy," IEEE Transactions on Biomedical Engineering, vol. 58, pp. 664-673, 2011.
7. M. M. Fraz, P. Remagnino, A. Hoppe, B. Uyyanonvara, A. R. Rudnicka, C. G. Owen, *et al*., "An ensemble classification-based approach applied to retinal blood vessel segmentation," IEEE Transactions on Biomedical Engineering, vol. 59, pp. 2538-2548, 2012.
8. S. W. Franklin and S. E. Rajan, "Diagnosis of diabetic retinopathy by employing image processing technique to detect exudates in retinal images," IET Image processing, vol. 8, pp. 601-609, 2014.
9. T. Mapayi, S. Viriri, and J.-R. Tapamo, "Comparative study of retinal vessel segmentation based on global thresholding techniques," *Computational and mathematical methods in medicine*, vol. 2015, 2015.
10. D. Wu, M. Zhang, J.-C. Liu, and W. Bauman, "On the adaptive detection of blood vessels in retinal images," IEEE Transactions on Biomedical Engineering, vol. 53, pp. 341-343, 2006.
11. J. Nayak, P. S. Bhat, R. Acharya, C. M. Lim, and M. Kagathi, "Automated identification of diabetic retinopathy stages using digital fundus images," *Journal of medical systems,* vol. 32, pp. 107-115, 2008.
12. P. K. R. Yelampalli, J. Nayak, and V. H. Gaidhane, "Blood Vessel Segmentation and Classification of Diabetic Retinopathy Images using Gradient Operator and Statistical Analysis," in Proceedings of the World Congress on Engineering and Computer Science, 2017.
13. S. Morales, V. Naranjo, J. Angulo, A. Legaz-Aparicio, and R. Verdú-Monedero, "Retinal network characterization through fundus image processing: Significant point identification on vessel centerline," Signal Processing: Image Communication, 2017.
14. U. T. Nguyen, A. Bhuiyan, L. A. Park, and K. Ramamohanarao, "An effective retinal blood vessel segmentation method using multi-scale line detection," Pattern recognition, vol. 46, pp. 703-715, 2013.
15. L. Chen, X. Huang, and J. Tian, "Retinal image registration using topological vascular tree segmentation and bifurcation structures," *Biomedical Signal Processing and Control,* vol. 16, pp. 22-31, 2015.
16. K. Chauhan and R. Gulati, "Pre-processing of retinal image and image segmentation using OTSU histogram," *Int. J. Adv. Inf. Sci. Technol.(*IJAIST), vol. 29, p. 29, 2014.
17. S. Karimi and H. Pourghassem, "Optical disc detection in retinal image based on spatial density of grayscale pixels," *International Journal of Imaging and Robotics*™, vol. 16, pp. 105-117, 2016.
18. Q. Li, B. Feng, L. Xie, P. Liang, H. Zhang, and T. Wang, "A cross-modality learning approach for vessel segmentation in retinal images," IEEE transactions on medical imaging, vol. 35, pp. 109-118, 2016.
19. J. Odstrcilik, R. Kolar, A. Budai, J. Hornegger, J. Jan, J. Gazarek, *et al*., "Retinal vessel segmentation by improved matched filtering: evaluation on a new high-resolution fundus image database," IET Image Processing, vol. 7, pp. 373-383, 2013.
20. Y. Q. Zhao, X. H. Wang, X. F. Wang, and F. Y. Shih, "Retinal vessels segmentation based on level set and region growing," *Pattern Recognition*, vol. 47, pp. 2437-2446, 2014.
21. G. Azzopardi and N. Petkov, "Automatic detection of vascular bifurcations in segmented retinal images using trainable COSFIRE filters," Pattern Recognition Letters, vol. 34, pp. 922-933, 2013.
22. K. Jiang, Z. Zhou, X. Geng, X. Zhang, L. Tang, H. Wu, *et al*., "Isotropic undecimated wavelet transform fuzzy algorithm for retinal blood vessel segmentation," *Journal of Medical Imaging and Health Informatics*, vol. 5, pp. 1524-1527, 2015.
23. S. W. Franklin and S. E. Rajan, "Retinal vessel segmentation employing ANN technique by Gabor and moment invariants-based features," *Applied Soft Computing,* vol. 22, pp. 94-100, 2014.
24. J. I. Orlando and M. Blaschko, "Learning fully-connected CRFs for blood vessel segmentation in retinal images," in International Conference on Medical Image Computing and Computer-Assisted Intervention, 2014, pp. 634-641.
25. D. Mahapatra, "Combining multiple expert annotations using semi-supervised learning and graph cuts for medical image segmentation," Computer Vision and Image Understanding, vol. 151, pp. 114-123, 2016.
26. J. Zhang, B. Dashtbozorg, E. Bekkers, J. P. Pluim, R. Duits, and B. M. ter Haar Romeny, "Robust retinal vessel segmentation via locally adaptive derivative

frames in orientation scores," IEEE transactions on medical imaging, vol. 35, pp. 2631-2644, 2016.
27. T. Kauppi, V. Kalesnykiene, J.-K. Kamarainen, L. Lensu, I. Sorri, A. Raninen, *et al*. (2007). DIARETDB1 - Standard Diabetic Retinopathy Database. Available: http://www.it.lut.fi/project/imageret/diaretdb1/
28. R. C. Gonzalez and R. E. Woods, "Processing," ed: Prentice-Hall, 2002.
29. R. C. Gonzalez and R. E. Woods, "Digital image processing," ed: Addison-wesley Reading, 1992.
30. J. K. Kristinsson, M. S. Gottfredsdóttir, and E. Stefánsson, "Retinal vessel dilatation and elongation precedes diabetic macular oedema," *British journal of ophthalmology*, vol. 81, pp. 274-278, 1997.
31. B. Liesenfeld, E. Kohner, W. Piehlmeier, S. Kluthe, S. Aldington, M. Porta, *et al*., "A telemedical approach to the screening of diabetic retinopathy: digital fundus photography," *Diabetes Care,* vol. 23, pp. 345-348, 2000.
32. J. Kittler, "On the accuracy of the Sobel edge detector," Image and Vision Computing, vol. 1, pp. 37-42, 1983.
33. P. Panchal, R. Bhojani, and T. Panchal, "An Algorithm for Retinal Feature Extraction using Hybrid Approach," Procedia Computer Science, vol. 79, pp. 61-68, 2016.
34. W. Gonzalez and R. E. Woods, "Eddins, Digital Image Processing Using MATLAB," Third New Jersey: Prentice Hall, 2004.
35. P. Soille, Morphological image analysis: principles and applications: Springer Science & Business Media, 2013.
36. R. Verd-Monedero, J. Angulo, and J. Serra, "Anisotropic morphological filters with spatially-variant structuring elements based on image-dependent gradient fields," IEEE Transactions on Image Processing, vol. 20, pp. 200-212, 2011.
37. R. S. Choras, "Image feature extraction techniques and their applications for CBIR and biometrics systems," *International journal of biology and biomedical engineering*, vol. 1, pp. 6-16, 2007.
38. Q. Zhu, Q. Feng, J. Huang, and D. Zhang, "Sparse representation classification based on difference subspace," in Evolutionary Computation (CEC), 2016 IEEE Congress on, 2016, pp. 4244-4249.
39. J. Staal, M. D. Abràmoff, M. Niemeijer, M. A. Viergever, and B. Van Ginneken, "Ridge-based vessel segmentation in color images of the retina," IEEE transactions on medical imaging, vol. 23, pp. 501-509, 2004.
40. D. Calvo, M. Ortega, M. G. Penedo, and J. Rouco, "Automatic detection and characterisation of retinal vessel tree bifurcations and crossovers in eye fundus images," Computer methods and programs in biomedicine, vol. 103, pp. 28-38, 2011.
41. C. I. Sánchez, M. Niemeijer, A. V. Dumitrescu, M. S. Suttorp-Schulten, M. D. Abramoff, and B. van Ginneken, "Evaluation of a computer-aided diagnosis system for diabetic retinopathy screening on public data," *Investigative ophthalmology & visual science*, vol. 52, pp. 4866-4871, 2011.
42. C. Agurto, V. Murray, E. Barriga, S. Murillo, M. Pattichis, H. Davis, *et al*., "Multiscale AM-FM methods for diabetic retinopathy lesion detection," IEEE transactions on medical imaging, vol. 29, pp. 502-512, 2010.
43. B. Antal and A. Hajdu, "An ensemble-based system for microaneurysm detection and diabetic retinopathy grading," IEEE transactions on biomedical engineering, vol. 59, pp. 1720-1726, 2012.
44. E. S. Barriga, V. Murray, C. Agurto, M. Pattichis, W. Bauman, G. Zamora, *et al*., "Automatic system for diabetic retinopathy screening based on AM-FM, partial least squares, and support vector machines," in Biomedical Imaging: From Nano to Macro, 2010 IEEE International Symposium on, 2010, pp. 1349-1352.
45. S. Roychowdhury, D. D. Koozekanani, and K. K. Parhi, "DREAM: diabetic retinopathy analysis using machine learning," IEEE journal of biomedical and health informatics, vol. 18, pp. 1717-1728, 2014.
46. G. Zhang, X. Shu, Z. Liang, Y. Liang, S. Chen, and J. Yin, "Multi-instance learning for skin biopsy image features recognition," in IEEE International Conference on Bioinformatics and Biomedicine (BIBM), 2012, pp. 1-6.

How to cite this article:

Ashok Kumar, D and Sankari, A.2018, A Hybrid Retinal Image Segmentation and Classification Approach for Diagnosis of Diabetic Retinopathy. *Int J Recent Sci Res.* 9(4), pp. 25812-25821. DOI: http://dx.doi.org/10.24327/ijrsr.2018.0904.1936

****